Journal of Materials Chemistry C

PAPER

View Article Online
View Journal | View Issue

Cite this: J. Mater. Chem. C, 2016, 4, 581

Color-tunable photoluminescence of Cu-doped Zn–In–Se quantum dots and their electroluminescence properties†

Sheng Cao,[ab] Wenyu Ji,[c] Jialong Zhao,[d] Weiyou Yang,[b] Chengming Li*[a] and Jinju Zheng*[b]

Received 28th November 2015,
Accepted 7th December 2015

DOI: 10.1039/c5tc04019a

www.rsc.org/MaterialsC

Recently, Cu-doped ternary chalcogenide quantum dots (QDs) have attracted extensive attention due to their large Stokes shift and tunable photoluminescence (PL) behavior in the visible and near-infrared (NIR) spectral range, and particularly for their remarkably lower toxicity than their Cd-based counterparts. However, there still remain material- and fabrication-related obstacles in realizing high-performance Cu-doped QDs, which limit their promising applications in light-emitting devices and bio-labeling. In the present study, we report the facile synthesis of high-qualified Cu-doped Zn–In–Se QDs *via* a hot injection approach, using a heterogeneous dispersion of Se in octadecene (ODE) as a "green" Se precursor. With variation of the ratios of Zn to In, the obtained Cu-doped Zn–In–Se QDs exhibited composition-tunable PL emissions over the most visible spectral window (*ca.* 565–710 nm) with a PL quantum yield (QY) up to 38% after coating ZnSe shells, which is the highest one ever reported in this system. Furthermore, we report, for the first time, the exploration of QD light-emitting diodes (QD-LEDs) based on the Cu-doped Zn–In–Se QDs as the active layer, which had a maximum luminance of 320 cd m^{-2} and a luminous efficiency (LE) of 0.97 cd A^{-1} (at 98 cd m^{-2}), suggesting their promising potential for application in optoelectronic devices.

Introduction

Transition metal ion-doped semiconductor quantum dots (QDs), as a novel type of luminescent material, not only retain nearly all the intrinsic advantages of QDs, but also possess additional merits such as large Stokes shift (to avoid self-absorption/energy transfer), enhanced thermal and chemical stability, as well as long excited state lifetimes, making them a potentially excellent candidate to be applied in biomedical diagnosis, solar cells, and light-emitting diodes (LEDs).[1–7] Among these doped nanocrystal (NC) emitters, the representative one is Mn-doped zinc chalcogenide, which shows stable and efficient emission with a photoluminescence quantum yield (PL QY) above 50%.[1,2] Because the dopant emission is considered to originate from the intrinsic $^4T_1$–$^6A_1$ transition of the Mn^{2+} ion, the emission wavelength from these doped QDs is generally limited within the yellow-orange spectral range (*i.e.*, 580–600 nm), which will greatly restrict the scope of their applications. Compared to the Mn dopants, the Cu species give a much wider range with tunable emission over the whole visible-NIR window depending on the size and composition of the host QDs.[1] According to the reported studies, the Cu-doped ZnS QDs often have green emission,[8] and the Cu-doped ZnSe counterparts show slightly more extension into the greenish-yellow spectral window,[9–11] and the doped CdS and InP QDs exhibit orange-red[12] and near-infrared ranges, respectively.[13]

A recent interesting finding is that the semiconductor materials of ternary chalcogenide compound NCs can be considered as one of the very promising alternatives to serve as the doping hosts, because they display composition-tunable electronic and optical properties.[1] For example, Cu-doped Zn–Cd–S alloyed QDs show emissions over nearly the complete visible window (440–710 nm).[14,15] However, unfortunately, such ternary alloyed QDs have doubtful application prospects, due to inclusion of the toxic element Cd. Recently, a Cd-free and Cu-doped Zn–In–S system has been developed, which shows a high PL QY and its emission covers the entire visible spectral window. In addition, a high maximum luminance of 220 cd m^{-2} in QD-LEDs made

[a] Institute for Advanced Materials and Technology, University of Science and Technology Beijing, Beijing 100083, China. E-mail: chengmli@mater.ustb.edu.cn; Fax: +86-574-87081221; Tel: +86-574-87080966
[b] Institute of Materials, Ningbo University of Technology, Ningbo 315016, China. E-mail: zhengzhao2007@163.com
[c] State Key Laboratory of Luminescence and Applications, Changchun Institute of Optics, Fine Mechanics and Physics, Chinese Academy of Sciences, Changchun 130033, China
[d] Key Laboratory of Functional Materials Physics and Chemistry of the Ministry of Education, Jilin Normal University, Siping 136000, China

† Electronic supplementary information (ESI) available: The structural characterizations and optical performances of the Cu-doped Zn–In–Se QDs. See DOI: 10.1039/c5tc04019a

from these Cu-doped Zn–In–S QDs was accomplished, suggesting their promising potential as less toxic NCs to be applied in LEDs.[16] Generally, compared to the metal sulfide QDs, the metal selenide ones have a higher valance band,[17] which could improve the hole injection efficiency from commonly used hole transfer materials to the QDs, thus it can be expected to further improve the performance of QD-LEDs. With respect to the state-of-the-art Cu-doped Zn–In–Se QDs, regardless of the fact that the obtained dopant Cu emission covers a 120 nm (*i.e.*, 540–660 nm) wavelength range with a promising emission efficiency of 20–30%,[18,19] there still remain material- and fabrication-related obstacles in realizing high-performance Cu-doped Zn–In–Se QDs, *e.g.*, the use of toxic and expensive Se–organophosphine complexes[18] and heating of Se powders in octadecene (ODE) under a protective atmosphere for a long time (up to 30 min) for the preparation of the Se precursor.[19] In addition, to date, little attention has been paid to the opto/electronic applications (especially in LEDs) of the Cu-doped Zn–In–Se QDs.

Herein, we applied a heterogeneous dispersion of Se in ODE as a "green" Se precursor to obtain an emission-tunable PL of Cd-free, Cu-doped Zn–In–Se QDs. By tailoring the Zn/In molar ratios through varying the ratios of zinc and indium reagents, color-tunable PL emissions over nearly complete visible spectral window (*ca.* 565–710 nm) were accomplished with a PL QY of up to 38%. The band gaps and energy levels were estimated by cyclic voltammetry (CV) analysis. Furthermore, the exploration of QD-LEDs based on our Cu-doped Zn–In–Se QDs was demonstrated *via* a full solution process. The as-built QD-LEDs exhibit high brightness and efficiency with a maximum luminance of 320 cd m^{-2} and luminous efficiency (LE) of 0.97 cd A^{-1} (at 98 cd m^{-2}). To the best of our knowledge, this is the first time that Cu-doped Zn–In–Se QDs have been used for the exploration of QD-LEDs with high performance.

Experimental section

Raw materials

Cuprous chloride (CuCl, 99.999%), sulfur powder (S, 99.99%), 1-dodecanethiol (DDT, 98%), oleylamine (OLA, 70%), and tetrabutylammonium hexafluorophosphate ($TBAPF_6$, 98%) were obtained from Aladdin Co, Ltd, China, and 1-octadecene (ODE, 90%) was obtained from Adamas-Beta Ltd, China. Zinc acetate ($Zn(Ac)_2$), indium(III) acetate ($In(Ac)_3$, 99.99% trace metals basis), and selenium (200 mesh, 99.999%) were purchased from Aldrich Co., USA. Poly(ethylenedioxythiophene):polystyrene sulphonate (PEDOT:PSS) and poly(*N*,*N*′-bis(4-butylphenyl)-*N*,*N*′-bis(phenyl)-benzidine) (poly-TPD) were purchased from Xi'an Polymer Light Technology Corp., China. All the chemicals were used directly without further purification.

Preparation of stock solutions

A typical Se stock solution (Se-SUS) was prepared by dispersing Se powder (63 mg, 0.8 mmol) in 1 mL ODE + 1 mL OLA by sonication for 5 min without any heating.

The zinc stock solution (0.1 M) for ZnSe shell growth was prepared by dissolving 183 mg (1 mmol) of $Zn(Ac)_2$ in a mixed solvent containing 8.0 mL of ODE and 2.0 mL of OLA at 50 °C in air. The obtained Zn stock solution was stored at 30 °C for subsequent use.

Synthesis of Cu-doped Zn–In–Se QDs

In a typical synthesis, CuCl (4 mg, 0.04 mmol), $In(Ac)_3$ (58 mg, 0.2 mmol), $Zn(Ac)_2$ (36 mg, 0.2 mmol), DDT (1 mL), OLA (1 mL) and ODE (5 mL) were loaded into a 100 mL three neck flask, and degassed for 20 min by bubbling with Ar at 100 °C. The temperature was further increased to the desired temperature of 200 °C, and the Se stock solution was injected quickly into the flask to form Cu-doped Zn–In–Se nanoclusters. The solution was then annealed for 30 min. Subsequently, the temperature was fixed at 200 °C and 1 mL of Zn stock solution was introduced into the reaction mixture followed by further annealing for 30 min. The resultant colloidal solution was allowed to cool naturally to room temperature (RT), and then purified repeatedly using methanol/hexane and precipitated using acetonitrile.

In the present experiment, Cu-doped Zn–In–Se core QDs with Zn/In composition ratios of 7 : 3, 5 : 5, 4 : 6, and 3 : 7 were synthesized by fixing the total amount of In and Zn precursors at 0.4 mmol. After overcoating the ZnSe shells *in situ* on the core, the resulting Cu-doped Zn–In–Se QDs were referred to as samples 1, 2, 3, and 4, respectively. The experimental results suggested that the production of the QDs *via* the present hot-injection strategy was highly repeatable.

Fabrication and characterization of QD-LEDs

QD-LEDs were fabricated on glass substrates coated with ITO. The substrates were cleaned consecutively with deionized water, acetone and isopropanol for 15 min each, and then treated for 10 min with ozone generated by the ultraviolet light in air. The substrates were then spin-coated with multiple layers in the order of: PEDOT:PSS, poly-TPD, Cu-doped Zn–In–Se QDs, and ZnO nanoparticles (NPs). The PEDOT:PSS solutions were spin-coated onto the ITO-coated glass substrates at 3000 rpm for 60 s and then baked at 150 °C for 10 min followed by spin-coating of poly-TPD (1.5 wt%, chlorobenzene), QDs (10 mg mL^{-1}, toluene) and ZnO NPs (30 mg mL^{-1}, ethanol) layers, which were then baked at 70 °C for 15 min. The spin speeds were fixed at 2500 and 2000 rpm for the preparation of poly-TPD and QDs/ZnO NPs layers, respectively. Upon completion of the abovementioned preparation steps in air, the multilayer samples were then loaded into a custom high-vacuum deposition chamber (background pressure, $\sim 3 \times 10^{-3}$ Pa) to deposit the top Al cathode (100 nm thickness), which was patterned by an *in situ* shadow mask to form an active device area of 5 mm^2.

Structural characterization and optical property measurement.

The QDs thus obtained were characterized using transmission electron microscopy (TEM, JEM-2100F, JEOL, Japan) along with energy dispersive X-ray spectroscopy (EDX, Quantax-STEM, Bruker, Germany), X-ray diffraction (XRD, D8 Advance, Bruker,

Germany), X-ray photoelectron spectroscopy (XPS, Thermo ESCALAB 250XI, USA) and ICP optical emission spectrometry (ICP-OES, Ultima 2, Horiba Jobin Yvon, France). The fabricated QD-LEDs were characterized by field-emission scanning electron microscopy (FESEM, S4800, Hitachi, Japan).

The UV-vis measurements of the obtained QDs were performed on a UV-vis scanning spectrophotometer (U-3900, Hitachi, Japan). The PL spectra, PL QY, and PL decay curves were recorded using a Fluromax-4P spectrometer (Horiba Jobin Yvon, France) equipped with a quantum-yield accessory and a time-correlated single-photon-counting (TCSPC) spectrometer. A pulsed NanoLED (wavelength: 370 nm) was used as the excitation source for the PL decay measurements.

Cyclic voltammograms (CV) were recorded on an electrochemical workstation (CHI600, Chenhua, China) using the glassy carbon disc, Pt wire and Ag/Ag^+ (Ag wires with 0.01 M $AgNO_3$ in acetonitrile) as the working, counter and reference electrodes, respectively. 0.1 M $TBAPF_6$ dissolved in acetonitrile was employed as the supporting electrolyte. The working electrodes were polished, cleaned, and dried before the deposition of the NC samples. One drop of diluted QDs solution was deposited onto the surface of the working electrode to form a QDs film. The scan rate was set at 50 mV s^{-1}. During all the experiments, the electrolyte solutions were thoroughly deoxygenated by bubbling nitrogen gas (99.99%).

Electroluminescence (EL) spectra and current–voltage–luminance characteristics were measured using a Minolta Luminance Meter LS-110 and a programmable Keithley model 2400 power supply in the air at RT, respectively.

Results and discussion

Synthesis and optical properties of Cu-doped Zn–In–Se QDs

To date, in the case of metallic Se-based QDs synthesis, toxic, expensive Se–organophosphine complexes are still commonly used as the Se precursor. To meet the development of "green" chemistry, novel alternatives to Se–organophosphine precursors have been reported recently, including pre-reacting elemental Se with alkanes,[20] dissolving elemental Se in ODE using a long heating time to form Se-ODE solution,[21] mixing SeO_2 with ODE,[22] and dissolving Se in ODE in the presence of either $NaBH_4$[23] or aliphatic thiol.[24] Most recently, it was indicated that a suspension of fine Se powder in octadecene (Se-SUS) can be a versatile and convenient Se precursor for the synthesis of metal selenide NCs.[25,26] In the present study, we have followed such a strategy for the growth of high-qualified Cu-doped Zn–In–Se QDs based on the hot injection method. In a typical experiment, with the total amount of In and Zn precursors fixed at 0.4 mmol, a mixture of CuCl, $In(Ac)_3$, $Zn(Ac)_2$, DDT, and ODE was heated to 200 °C. The Se-SUS solution was then injected into the solution, and it was maintained at the injection temperature for the growth of QDs (see Experimental section).

Fig. 1 shows the UV-visible absorption and PL spectra of Cu-doped Zn–In–Se QDs with different nominal Zn/In precursor ratios. It is found that the Zn/In precursor ratios greatly influence the optical properties of the resultant doped QDs. As shown in Fig. 1a, the absorption onset of Cu-doped Zn–In–Se core QDs exhibit red-shifts systematically from 550 to 610 nm with the decrease in the nominal Zn : In precursor ratios from 7 : 3 to 3 : 7. As expected, the corresponding Cu dopant emission also makes a red-shift, nevertheless with a much more pronounced extension from 585 to 710 nm (Fig. 1a). Such color-tunable emission arises from the recombination of electrons in the conduction band of the host material with holes in the Cu T_2 state.[16,25,26] The corresponding PL excited-state lifetimes were measured to clarify the origin of the emissions. As shown in Fig. S1 (ESI†), the PL decay curves were fitted by the bi-exponential function. The longer lifetime of hundreds of nanoseconds can be attributed to dopant-related recombination, while the shorter lifetime of tens of nanoseconds can be ascribed to the recombination of defect-states, because the Zn/In ratio of all the samples deviates from their stoichiometric ratio.[1,2] The average PL excited-state lifetime falls in the range of 194–298 ns (see Fig. S1 and Table S2, ESI†), which suggests that this emission mainly originates from the Cu dopant transition. Thus, the color-tunable emission in samples with various Zn/In precursor ratios should arise from the recombination of electrons in the conduction band of the host material and holes in the Cu T_2 state, which are similar to the reported studies for Cu-doped QDs.[16,25,26]

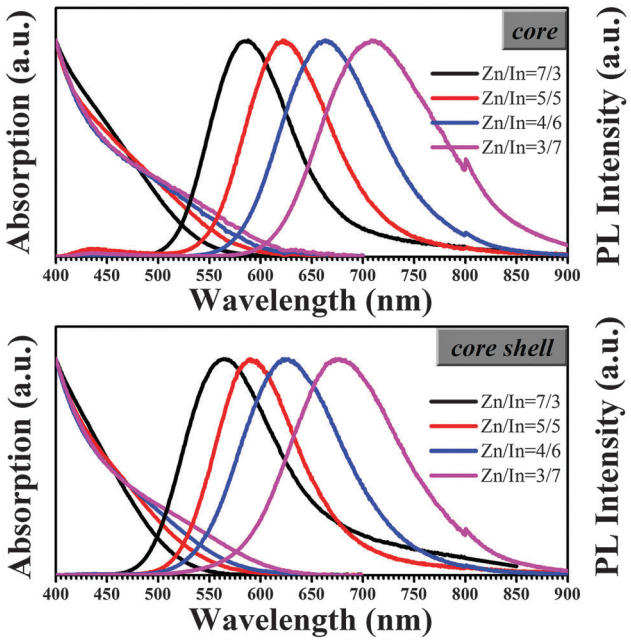

Fig. 1 UV-visible absorption (left) and PL spectra (right, λ_{ex}=365 nm) of Cu-doped Zn–In–Se core QDs (a) and Cu-doped Zn–In–Se core shell QDs (b) dispersed in chloroform prepared under various nominal Zn/In precursor molar ratios.

To improve the PL QY and stability of the Cu-doped Zn–In–Se QDs, the Cu-doped Zn–In–Se–ZnSe core–shell structures are constructed *via* the *in situ* formation in the crude Cu-doped Zn–In–Se core reaction solution with a growth time of 30 min.[27–29] With respect to the residual selenium source existing within the reaction mixture of Cu-doped Zn–In–Se core, no additional selenium source was added in the ZnSe shell deposition process.

Table 1 Detailed PL properties of Cu-doped Zn–In–Se QDs under different nominal Zn/In ratios

Nominal Zn/In ratios	Samples	Peak/nm	fwhm[a]/nm	PL QY/%
Zn/In = 7 : 3	Core	585	91	11
	Core–shell (sample 1)	565	107	23
Zn/In = 5 : 5	Core	621	96	18
	Core–shell (sample 2)	590	93	38
Zn/In = 4 : 6	Core	663	111	16
	Core–shell (sample 3)	621	115	35
Zn/In = 3 : 7	Core	710	132	16
	Core–shell (sample 4)	673	143	32

[a] fwhm refers to the full width at half maximum.

As shown in Fig. 1b, with the overgrowth of the ZnSe shell around the Cu-doped Zn–In–Se cores, the PL peak positions blue-shift slightly from the initial 585, 621, 663 and 710 nm to 565, 590, 621 and 673 nm, for samples 1, 2, 3 and 4, respectively. More detailed PL properties of the core and corresponding core–shell samples are summarized in Table 1. Generally, the blue-shift of the PL peak position induced by the ZnSe overcoating process indicates the further incorporation of the zinc component into the core material, resulting in an increase in the band gap energy.[18,19] Moreover, the resulting PL QY increases substantially, with the optimized absolute PL QYs up to ~38%, which is the highest ever reported in this system.[18,19] Their chemical composition characterizations by EDX and ICP-OES (Table S1, Fig. S2 and Table S3, ESI†) reveal that the real Zn/In ratios in the final core samples are much lower than the nominal values, which might be due to the different chemical reactivity of Zn and In precursors. In addition, the Zn component in the corresponding core–shell samples increases clearly relative to their cores, indicating the successful overcoating of the ZnSe shells around the cores.

For the synthesis of ternary metal selenide NCs, apart from the inherent difficulty with the Se precursor, there is another problem of balancing the reactivity of these cations/anions in the reaction solution.[7,16,30,31] In our case, we make use of a strongly coordinating chemical reagent, namely DDT, as the capping ligand to accomplish this balance. As shown in Fig. 1, with the decrease in the nominal Zn/In precursor ratios from 7 : 3 to 3 : 7, a systematic red-shift is observed in the resultant ternary NCs. This indicates that the homogeneous Zn–In–Se host NCs should be formed *via* intermixing of the wider band gap of ZnSe (2.7 eV) with the narrower band gap of InSe (1.8 eV),[18] rather than the formation of separate ZnSe and InSe NCs. This could be due to the fact that once ZnSe or InSe nucleates separately, the corresponding absorption lines should have various contours instead of gradually shift from ~550 to ~610 nm (Fig. 1).

To further reveal the optical properties of the obtained QDs, 2D-PLE maps are used in which the PL intensities as a function of excitation wavelengths are recorded. Fig. 2(a–c) show the 2D-PLE maps from Cu-doped Zn–In–Se QDs with nominal Zn/In precursor molar ratios of 5 : 5 (sample 2), 4 : 6 (sample 3) and 3 : 7 (sample 4), respectively (similar data are not presented for the sample 1 due to the poor optical property of the QDs). The relative oscillator strength of Cu emission can be derived from the PLE spectra by tracing the landscape of the color changes. For all the samples, an obvious gap between excitation and emission caused by the Stokes shift can be observed. Furthermore, the PL spectra possess basically similar peak wavelengths at ~590, ~621, and ~673 nm for samples 2, 3 and 4, respectively, when excited at wavelengths ranging from 300 to 500 nm. These results imply that the local environment of emission centers should be the homogeneous host rather than ZnSe and/or InSe NCs.[7,31]

Morphology and structure of Cu-doped Zn–In–Se QDs

Fig. 3 shows the typical TEM images of the as-grown Cu-doped Zn–In–Se core–shell QDs with different nominal Zn/In precursor molar ratios. It appears that the resultant NCs appear to be nearly spherical in shape and fairly monodisperse. The lattice fringes could be observed clearly, indicating the formation of the NCs with some degree of regularity. The insets in Fig. 3 show the size distributions of the corresponding QDs, suggesting their average sizes of ~3.4, 3.2, 3.4 and 3.3 nm, corresponding to samples 1, 2, 3 and 4, respectively. These almost identical size QDs, regardless of the different Zn/In molar ratios, confirm that the tunable Cu ion emissions (as shown in Fig. 1) from the QDs do not derive from the well-recognized "size-dependent optical property", but rather are imposed by a "composition-dependent optical property",[16,18,26,32] implying that the tunable band gap energies and emission colors might find some special application such as in QD-LEDs and QD-sensitized solar cells.

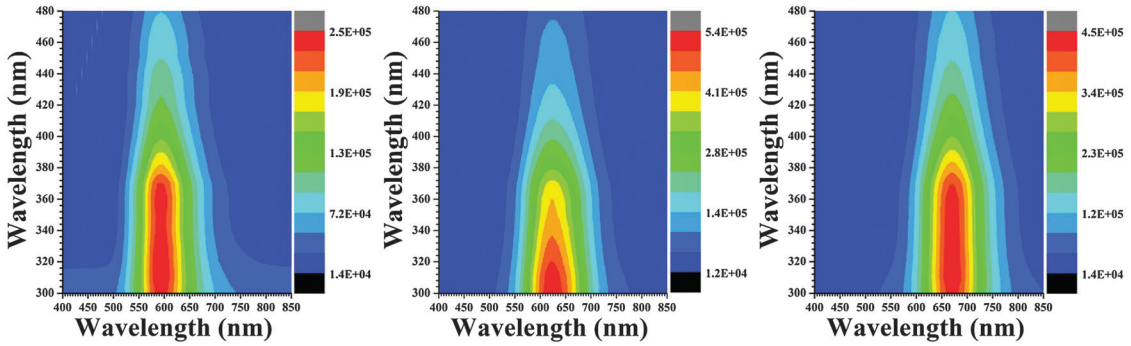

Fig. 2 (a–c) Typical 2D PLE maps of colloidal Cu-doped Zn–In–Se QDs under nominal Zn/In molar ratios of 5 : 5 (sample 2), 4 : 6 (sample 3), and 3 : 7 (sample 4) at room temperature, respectively. The intensity scales (colored contours) are in arbitrary units.

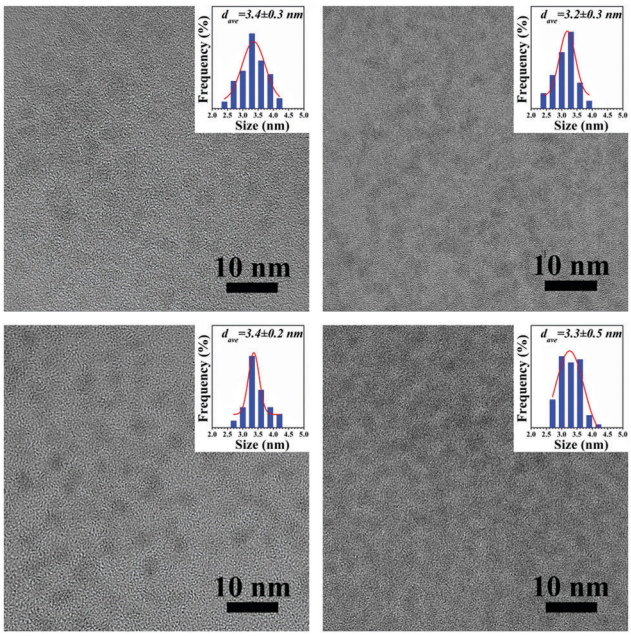

Fig. 3 Typical TEM images of the Cu-doped Zn–In–Se QDs with nominal Zn/In precursor molar ratios of 7 : 3 (a, sample 1), 5 : 5 (b, sample 2), 4 : 6 (c, sample 3), and 3 : 7 (d, sample 4). The insets show the size distributions of the corresponding QDs of samples 1–4.

Fig. 4 shows the typical XRD patterns of the four Cu-doped Zn–In–Se QD samples with different Zn/In precursor molar ratios. The XRD patterns for all the doped QD samples match well with the tetragonal $ZnIn_2Se_4$ crystal data (JCPDS no. 39-0458), indicating that the QDs should be a tetragonal phase of Zn–In–Se. The peaks shift systematically toward smaller angles as the Zn/In ratio decreases, owing to the substitution of smaller Zn^{2+} ions (r = 0.88 Å) by larger In^{3+} (r = 0.94 Å) ones.[18] The average diameters of the QDs are *ca.* 3.0, 3.1, 3.0 and 3.2 nm corresponding to samples 1, 2, 3 and 4, respectively, based on the Debye–Scherrer formula and the (111) peak position within the XRD pattern, which are in good agreement with the TEM observations. To further identify potential ZnSe binary impurities with similar XRD patterns to those of $ZnIn_2Se_4$, characterization by Raman spectroscopy was performed and the result is shown in Fig. S3 (ESI†). No detectable Raman peak at 351 cm^{-1} from ZnSe is found,[19,33] confirming the absence of ZnSe impurities.

The typical surface chemical compositions of Cu-doped Zn–In–Se QDs are determined through X-ray photoelectron spectroscopy (XPS) characterization. As shown in Fig. S4 (ESI†), the Cu-doped Zn–In–Se QDs with Zn/In precursor molar ratio of 5 : 5 (sample 2) represent the dominant photoelectron signals of Se 3d (at 54.1 eV), In 3d (at 443.8 and 451.4 eV), Cu 2p (at 931.3 and 951.2 eV) and Zn 2p (at 1021.4 and 1044.3 eV), confirming that the Se, In, Cu and Zn elements within the doped QDs are in their expected valences (Se^{2-}, In^{3+}, Cu^{+} and Zn^{2+}), as shown in Fig. S3a–d, respectively.[34]

Band gaps and energy levels of Cu-doped Zn–In–Se QDs

Fig. 5 shows the representative CV curves recorded on the dispersion of Cu-doped Zn–In–Se QDs at a scan rate of 50 mV s^{-1}, evidencing the characteristic gap or energy barrier in the middle of potential scan followed by asymmetric redox peaks (the typical CV curve of the electrolyte (blank) is shown in Fig. S5 (ESI†)). It is noted that the oxidation/reduction peaks of the NCs appear at slightly different potentials, suggesting variations in their chemical compositions and structures.[35–37] The onsets of oxidation and reduction peaks are marked by the short lines in Fig. 5. It shows that the oxidation potential moves to the negative side, and the reduction potential moves to the positive side for Cu-doped samples with the decrease of the Zn/In ratio. More specifically, all the sample peaks occur in the range of ~1.35–1.39 V (*vs.* Ag/Ag+) for oxidation and from ~−0.83 to −1.03 V for reduction. The energy levels of the conduction and valence band edges can be calculated from the peak oxidation potential (E^{ox}) and peak reduction potential (E^{red}), respectively, according to the following equations:[35,38]

$$E_{HOMO} = (E_{ox} + 4.71)\ eV \quad (1)$$

$$E_{LOMO} = -(E^{red} + 4.71)\ eV \quad (2)$$

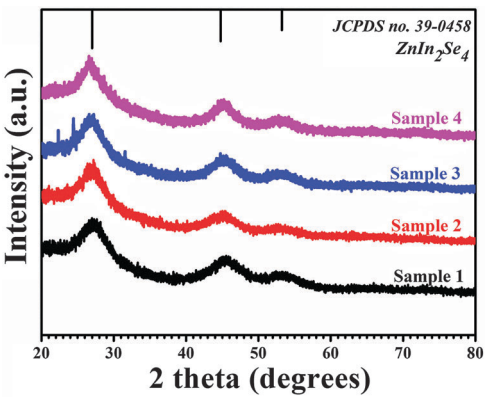

Fig. 4 Typical XRD patterns of the Cu-doped Zn–In–Se QDs with nominal Zn/In precursor molar ratios at 7 : 3 (black, sample 1), 5 : 5 (red, sample 2), 4 : 6 (blue, sample 3), and 3 : 7 (purple, sample 4). The vertical lines show the standard XRD pattern for tetragonal $ZnIn_2Se_4$ (JCPDS No. 39-0458).

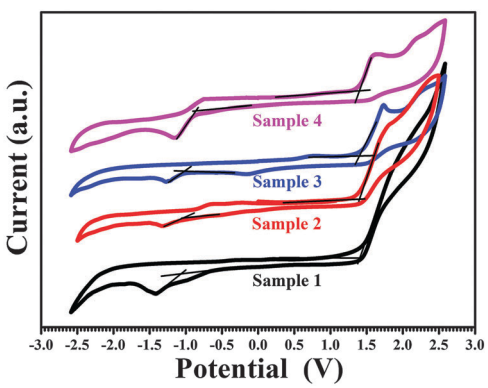

Fig. 5 Typical CV curves of Cu-doped Zn–In–Se QDs with nominal Zn/In precursor molar ratios of 7 : 3 (black, sample 1), 5 : 5 (red, sample 2), 4 : 6 (blue, sample 3), and 3 : 7 (purple, sample 4).

For the samples with various compositions of Zn and In, the band gaps (E_g) are 2.42, 2.37, 2.31 and 2.18 eV for samples 1, 2, 3 and 4 (as shown in Table 2). These values are in good agreement with the optical band gaps determined from the UV-vis absorption spectra, which correspond to the absorption bands at ~550–620 nm, as presented in Fig. 1b.

Fabrication of LEDs using Cu-doped Zn–In–Se QDs as emitters

Recently, excellent optoelectronic properties of Cd-free (*e.g.*, $CuInS_2$-based) QD-LEDs have been reported.[16,40,41] However, to the best of our knowledge, the EL of Cu-doped ternary metal selenide QDs has not yet been reported. Considering our high-qualified QDs with tunable PL emissions, we now shed light on the exploration of LEDs based on Cu-doped Zn–In–Se QDs, which have been fabricated using a fully solution-processed method (schematically shown in Fig. 6a). The as-fabricated QD-LEDs consist, sequentially, of the layers of ITO, PEDOT:PSS (35 nm), poly-TPD (30 nm), Cu-doped Zn–In–Se QDs (40 nm), ZnO NPs (30 nm) and Al (100 nm) (see the typical cross-section of the multilayer-structured QD-LED, shown in Fig. S6, ESI†). The poly-TPD and ZnO layers are selected as the hole-transporting layer (HTL) and electron-transporting (ETL) layer, respectively. All layers are spin-coated onto the patterned ITO substrates except for the Al cathode, which is deposited through vacuum thermal evaporation. The orthogonal solvents are used for adjacent layers to avoid physical damage to films caused by sequential casting processes in such multilayer structures.[42] The schematic energy level diagram of the QD-LEDs is shown in Fig. 6b. The ZnO nanoparticle (NP) layer is used to provide an efficient electron injection channel as well as a hole blocking layer due to the valence band offset at the QD/ZnO NP interface, leading to an improved efficiency of charge injection. The PL spectra of Cu-doped Zn–In–Se QDs, centered at 590 nm (sample 2), 621 nm (sample 3) and 673 nm (sample 4), as well as the EL spectra of the corresponding QD-LEDs, are shown in Fig. 6c. Their PL and the corresponding EL spectra have similar line shapes, and no noticeable parasitic emission is observed from the adjacent organic layers in the EL spectra, verifying that the emissions are mainly derived from the Cu-doped Zn–In–Se QDs. It is observed

Table 2 Electrochemical properties of the four Cu-doped Zn–In–Se QD samples

	E^{ox}/V	E^{red}/V	HOMO/eV	LOMO/eV	E_g/eV
Sample 1	1.39	−1.03	−6.10	−3.68	2.42
Sample 2	1.37	−1.00	−6.08	−3.71	2.37
Sample 3	1.35	−0.96	−6.06	−3.75	2.31
Sample 4	1.35	−0.83	−6.06	−3.88	2.18

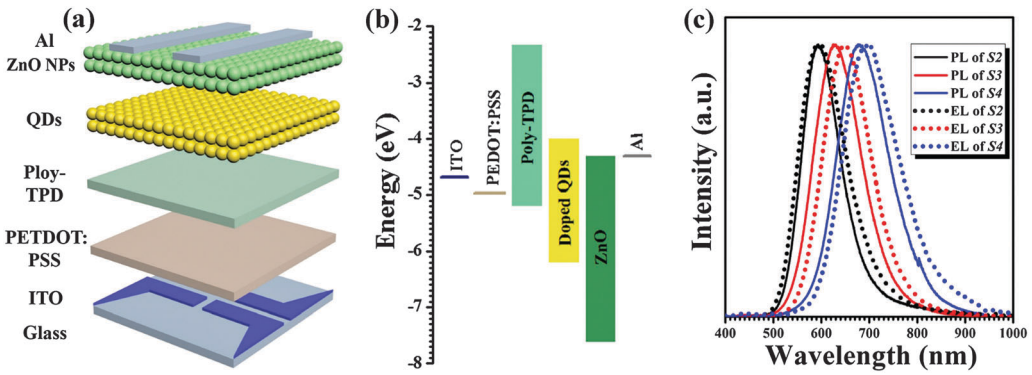

Fig. 6 (a) Schematic illustration of fabricated QD-LED device. (b) The energy level diagram for the various layers within the QD-LED device cited from the literature.[39] (c) Normalized PL (solid lines) and the corresponding EL (dashed lines) spectra of Cu-doped Zn–In–Se QDs for samples 2, 3 and 4.

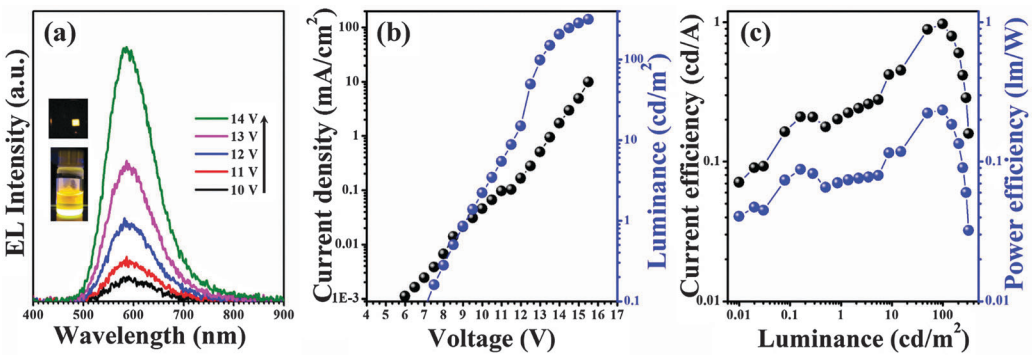

Fig. 7 A typical EL performance of a QD-LED based on sample 2. (a) Evolution of the EL spectra for the QD-LED at various voltages. (b) Current density and luminance of the devices *vs.* driving voltage. (c) Current efficiency and power efficiency *vs.* luminance. The insets in (a) are (upper) EL image under an operating voltage of 12 V and (lower) picture of QDs in solution under the radiation of a UV lamp.

that the EL spectra shift slightly to a longer wavelength and are broadened compared to their solution PL spectra in chloroform (the detailed comparison between the PL and EL spectra are summarized in Table S4, ESI†), which are similar to the previous reports.[16,30,40,43–45] Generally, they could be mainly attributed to following two cases: one is the Förster energy transfer from a small QD to a large one in the close-packed QD solids, and the other is the quantum-confined Stark effect due to polarization fields.[40,43] However, in our case, the doped QDs which, with large Stokes shifts, should have negligible Förster energy transfer process because the spectral overlap integral between acceptor absorption and donor emission is very small. Thus, the quantum-confined Stark effect might play a dominate role in the red-shift behavior.

Fig. 7 shows typical EL performance of a QD-LED based on sample 2 as an active layer. As shown in Fig. 7a, with the increase in the operating voltage, the intensities of the EL emission are generally enhanced and the spectral shape and peak position show no distinguishable differences. The evolutions of the EL data for the QD-LEDs based on samples 3 and 4 at various voltages are shown in Fig. S7 (ESI†), and the EL is undetectable for the QD-LED based on sample 1 due to its poor PL properties. Fig. 7b presents the luminance–current–voltage (*L–I–V*) characteristics of the QD-LED device. It shows that the turn-on voltage (V_{on}) is about 7 V, which is higher than those of other QD-LEDs. This could be mainly attributed to the fact that the current LEDs have been fabricated without the optimization of film quality.[16] It is found that the maximum QD-LED luminance can reach 320 cd m^{-2} (at 15 V). Once fixed at an injection current density of 0.51 mA cm^{-2} (*i.e.*, brightness of 98 cd m^{-2}), the as-fabricated QD-LED exhibits a luminous efficiency (LE) of 0.97 cd A^{-1} and a power efficiency (PE) of 0.23 lm W^{-1} (Fig. 7c), which are higher than those of other CuInSe-based QD-LEDs.[30] However, compared to those of well-developed CdSe-based counterparts, the efficiency is still much lower, which might be attributed to the unbalanced electron and hole injection or high resistance of the NC layer caused by the presence of the insulating ligands.[46–48] Nevertheless, the preliminary results for our QD-LEDs are still inspiring, because no structural optimization has yet been performed for the device.

Conclusions

In summary, we have demonstrated a facile ''green'' method for the synthesis of emission-tunable Cu-doped Zn–In–Se QDs, using a heterogeneous dispersion of Se in ODE as a ''green'' Se precursor. Through varying the composition of Zn–In–Se alloyed NCs under identical particle size, the as-synthesized Cu-doped Zn–In–Se QDs exhibit color-tunable PL emissions, which cover most of the visible range (*ca.* 565–710 nm) with a PL QY up to 38%. Furthermore, the as-fabricated LEDs based on the Cu-doped Zn–In–Se QDs exhibit high brightness with a maximum luminance of 320 cd m^{-2} and a luminous efficiency (LE) of 0.97 cd A^{-1} (at 98 cd m^{-2}). These results show the very promising potential of our Cu-doped Zn–In–Se QDs as excellent candidates for the exploration of novel and efficient QD-LED devices *via* an environmentally-friendly preparative route.

Acknowledgements

This study was financially supported by the National Natural Science Foundation of China (NSFC, Grant No. 61106066), Zhejiang Provincial Science Foundation (Grant No. LY14F040001) and Ningbo Municipal Natural Science Foundation (Grant No. 2015A610241).

References

1 P. Wu and X.-P. Yan, *Chem. Soc. Rev.*, 2013, **42**, 5489–5521.
2 N. Pradhan and D. Sarma, *J. Phys. Chem. Lett.*, 2011, **2**, 2818–2826.
3 P. K. Santra and P. V. Kamat, *J. Am. Chem. Soc.*, 2012, **134**, 2508–2511.
4 L. R. Bradshaw, K. E. Knowles, S. McDowall and D. R. Gamelin, *Nano Lett.*, 2015, **15**, 1315–1323.
5 X. Yuan, R. Ma, W. Zhang, J. Hua, X. Meng, X. Zhong, J. Zhang, J. Zhao and H. Li, *ACS Appl. Mater. Interfaces*, 2015, **7**, 8659–8666.
6 Z. Zhang, S. Luan, K. Huang, Y. Zhang, Z. Shi, R. Xie and W. Yang, *J. Mater. Chem. C*, 2015, **3**, 3614–3622.
7 S. Cao, C. Li, L. Wang, M. Shang, G. Wei, J. Zheng and W. Yang, *Sci. Rep.*, 2014, **4**, 7510.
8 J. Huang, Y. Yang, S. Xue, B. Yang, S. Liu and J. Shen, *Appl. Phys. Lett.*, 1997, **70**, 2335–2337.
9 S. Gul, J. K. Cooper, C. Corrado, B. Vollbrecht, F. Bridges, J. Guo and J. Z. Zhang, *J. Phys. Chem. C*, 2011, **115**, 20864–20875.
10 C. Wang, S. Xu, Z. Wang and Y. Cui, *J. Phys. Chem. C*, 2011, **115**, 18486–18493.
11 S. Jana, B. B. Srivastava, S. Acharya, P. K. Santra, N. R. Jana, D. Sarma and N. Pradhan, *Chem. Commun.*, 2010, **46**, 2853–2855.
12 A. Tang, L. Yi, W. Han, F. Teng, Y. Wang, Y. Hou and M. Gao, *Appl. Phys. Lett.*, 2010, **97**, 033112.
13 R. Xie and X. Peng, *J. Am. Chem. Soc.*, 2009, **131**, 10645–10651.
14 W. Zhang, X. Zhou and X. Zhong, *Inorg. Chem.*, 2012, **51**, 3579–3587.
15 B. B. Srivastava, S. Jana and N. Pradhan, *J. Am. Chem. Soc.*, 2010, **133**, 1007–1015.
16 W. Zhang, Q. Lou, W. Ji, J. Zhao and X. Zhong, *Chem. Mater.*, 2013, **26**, 1204–1212.
17 P. Reiss, M. Proti''re and L. Li, *Small*, 2009, **5**, 154–168.
18 S. Sarkar, N. S. Karan and N. Pradhan, *Angew. Chem., Int. Ed.*, 2011, **50**, 6065–6069.
19 J. Ke, X. Li, Q. Zhao, Y. Shi and G. Chen, *Nanoscale*, 2014, **6**, 3403–3409.
20 Z. Deng, L. Cao, F. Tang and B. Zou, *J. Phys. Chem. B*, 2005, **109**, 16671–16675.
21 J. Jasieniak, C. Bullen, J. van Embden and P. Mulvaney, *J. Phys. Chem. B*, 2005, **109**, 20665–20668.
22 O. Chen, X. Chen, Y. Yang, J. Lynch, H. Wu, J. Zhuang and Y. C. Cao, *Angew. Chem., Int. Ed.*, 2008, **47**, 8638–8641.
23 Y. Wei, J. Yang, A. W. H. Lin and J. Y. Ying, *Chem. Mater.*, 2010, **22**, 5672–5677.

24 Y. Liu, D. Yao, L. Shen, H. Zhang, X. Zhang and B. Yang, *J. Am. Chem. Soc.*, 2012, **134**, 7207–7210.
25 C. Pu, J. Zhou, R. Lai, Y. Niu, W. Nan and X. Peng, *Nano Res.*, 2013, **6**, 652–670.
26 T. Aubert, M. Cirillo, S. Flamee, R. Van Deun, H. Lange, C. Thomsen and Z. Hens, *Chem. Mater.*, 2013, **25**, 2388–2390.
27 J. Zheng, S. Cao, L. Wang, F. Gao, G. Wei and W. Yang, *RSC Adv.*, 2014, **4**, 30948–30952.
28 J. Zheng, W. Ji, X. Wang, M. Ikezawa, P. Jing, X. Liu, H. Li, J. Zhao and Y. Masumoto, *J. Phys. Chem. C*, 2010, **114**, 15331–15336.
29 S. Cao, J. Zheng, J. Zhao, L. Wang, F. Gao, G. Wei, R. Zeng, L. Tian and W. Yang, *J. Mater. Chem. C*, 2013, **1**, 2540–2547.
30 H. Zhong, Z. Wang, E. Bovero, Z. Lu, F. C. van Veggel and G. D. Scholes, *J. Phys. Chem. C*, 2011, **115**, 12396–12402.
31 S. Cao, J. Zhao, W. Yang, C. Li and J. Zheng, *J. Mater. Chem. C*, 2015, **3**, 8844–8851.
32 R. E. Bailey and S. Nie, *J. Am. Chem. Soc.*, 2003, **125**, 7100–7106.
33 A. Singh, S. Singh, S. Levcenko, T. Unold, F. Laffir and K. M. Ryan, *Angew. Chem., Int. Ed.*, 2013, **52**, 9120–9124.
34 S. Li, Z. Zhao, Q. Liu, L. Huang, G. Wang, D. Pan, H. Zhang and X. He, *Inorg. Chem.*, 2011, **50**, 11958–11964.
35 H. Zhong, S. S. Lo, T. Mirkovic, Y. Li, Y. Ding, Y. Li and G. D. Scholes, *ACS Nano*, 2010, **4**, 5253–5262.
36 B. Chen, S. Chang, D. Li, L. Chen, Y. Wang, T. Chen, B. Zou, H. Zhong and A. L. Rogach, *Chem. Mater.*, 2015, **27**, 5949–5956.
37 G. B. Markad, S. Battu, S. Kapoor and S. K. Haram, *J. Phys. Chem. C*, 2013, **117**, 20944–20950.
38 Y. Yang, H. Zhong, Z. Bai, B. Zou, Y. Li and G. D. Scholes, *J. Phys. Chem. C*, 2012, **116**, 7280–7286.
39 M. D. Ho, D. Kim, N. Kim, S. M. Cho and H. Chae, *ACS Appl. Mater. Interfaces*, 2013, **5**, 12369–12374.
40 Z. Tan, Y. Zhang, C. Xie, H. Su, J. Liu, C. Zhang, N. Dellas, S. E. Mohney, Y. Wang and J. Wang, *Adv. Mater.*, 2011, **23**, 3553–3558.
41 B. Chen, H. Zhong, W. Zhang, Z. a. Tan, Y. Li, C. Yu, T. Zhai, Y. Bando, S. Yang and B. Zou, *Adv. Funct. Mater.*, 2012, **22**, 2081–2088.
42 L. Qian, Y. Zheng, J. Xue and P. H. Holloway, *Nat. Photonics*, 2011, **5**, 543–548.
43 Y. Shirasaki, G. J. Supran, W. A. Tisdale and V. Bulović, *Phys. Rev. Lett.*, 2013, **110**, 217403.
44 W. Ji, P. Jing, J. Zhao, X. Liu, A. Wang and H. Li, *Nanoscale*, 2013, **5**, 3474–3480.
45 J. W. Stouwdam and R. A. Janssen, *Adv. Mater.*, 2009, **21**, 2916–2920.
46 W. Ji, P. Jing, L. Zhang, D. Li, Q. Zeng, S. Qu and J. Zhao, *Sci. Rep.*, 2014, **4**, 6974.
47 W. Ji, Y. Tian, Q. Zeng, S. Qu, L. Zhang, P. Jing, J. Wang and J. Zhao, *ACS Appl. Mater. Interfaces*, 2014, **6**, 14001–14007.
48 K.-H. Lee, J.-H. Lee, W.-S. Song, H. Ko, C. Lee, J.-H. Lee and H. Yang, *ACS Nano*, 2013, **7**, 7295–7302.

